# Dynamic Instability of Thermal-Flying-Height-Control Sliders at Touchdown

Jinglin Zheng and David B. Bogy

Computer Mechanics Laboratory
Department of Mechanical Engineering,
University of California at Berkeley, Berkeley, CA 94720

**Abstract**

With the wide application of thermal flying-height control (TFC) technology in the hard disk drive industry, the head-disk clearance can be controlled to as low as ~1nm. At this ultra-low clearance, the air bearing slider is subject to relatively large interfacial forces, and it experiences more complicated dynamics, compared with the flying case. In this study we conduct a numerical analysis to investigate the dynamics of TFC sliders during touchdown. The general trend of the slider's motion predicted by the numerical simulation qualitatively agrees with experimental findings. The touchdown process begins with a slight intermittent contact between the slider's trailing edge and the disk, followed by a partial slider-disk contact at the trailing edge accompanied by a large pitch motion at the 1st air bearing mode; this pitch motion gets suppressed and the slider comes into stable sliding on the disk as the protrusion is further increased.

***Keywords:*** *thermal-flying-height-control, touchdown, air bearing, contact*

## Introduction

The application of thermal flying-height control (TFC) technology in hard disk drives allows the head-disk clearance to be controlled to as low as ~1nm. At this ultra-low clearance the air bearing slider is subject to relatively large interfacial forces, and it experiences more complicated dynamics, compared with the higher flying case (Canchi and Bogy 2010; Zeng et al. 2011; Su et al. 2011). Proper numerical modeling of the slider dynamics at this ultra-low physical clearance can provide useful tools for hard disk drive engineers to improve the head-disk interface design.

In this paper a numerical method is used to study the slider's touchdown dynamics at this ultra-low clearance. Slider instabilities that have been observed by others at a certain thermal actuation range can be predicted through this numerical procedure. More details regarding the unstable dynamics are revealed through further analysis of the numerical results.

## Numerical approach

This study uses a numerical approach to examine the slider's touchdown dynamics. The numerical method involves two essential steps: i) solving the air bearing equations for the air bearing pressure, and ii) solving the slider's dynamics that is subject to this pressure and interfacial forces. A femto-sized slider (0.85mm×0.70mm×0.23mm) with the air bearing design used in Zheng et al. (2009) is adopted for this study. The time-variant Reynolds equation is solved at each time step

to obtain the air bearing pressure. Various interfacial forces (intermolecular, electrostatic, contact, friction) are characterized using a sub-boundary lubrication model (Zheng and Bogy 2010; Stanley et al. 1990). The air bearing pressure loss due to head-disk contact is accounted for by following the multi-asperity approach adopted in the sub-boundary lubrication model. A 18mm-long, LDV (Laser Doppler Vibrometer)-measured disk profile (shown in Figure 1), is applied repeatedly on the disk to represent the moving waviness (Chen and Bogy 2007). An AFM (Atomic Force Microscope) measured slider-disk topography is used in the multi-asperity model for air bearing and interfacial force calculations (Chen and Bogy 2007). To bring the slider from flying to touchdown, a time-varying heater-induced bulge profile is applied onto the slider's surface to change the original air bearing geometry. Figure 2 shows the bulge profile used to modify the air bearing surface geometry, which originally has a peak of 10nm. This profile is increased proportionally to bring the slider from flying to touchdown.

**Result discussion**

An actuation profile as shown in Figure 3 is applied to the slider. The actuation profile goes up from 25nm to 45nm with a 1nm step. Each actuation step lasts for 1ms and the total length of the simulation time is 21ms.

Figure 4 shows the 3σ history of the slider's pitch motion during this actuation process. The pitch 3σ is low at the early actuation steps. It starts increasing rapidly at around the 30nm actuation. It then peaks at 33nm, and starts decreasing afterwards.

This non-monotonic trend of the slider's vibration amplitude during touchdown qualitatively agrees with some recent experimental findings in (Canchi and Bogy 2010; Zeng et al. 2011; Su et al. 2011).

Figure 5 shows the power spectrums of five representative actuation steps (25nm, 30nm, 33nm, 40nm, 45nm) obtained from fast Fourier transforms of the pitch histories. As the actuation increases from 25nm to 30nm, a few spikes appear at around 400kHz with the highest peak located at 435.6kHz. By locating the points on the slider having minimum vibration amplitude at this frequency, we are able to identify the nodal line for this specific vibration mode, which is shown in Figure 6. The nodal line is located at the central part of the slider, toward the leading edge, thus is considered to be the pitch axis of the 2nd air bearing mode. The history of the contact force (Figure 7) shows that the contact force abruptly increases at the 30nm actuation. Thus, the slider is brought into contact with the disk at its trailing edge at this actuation step. Note that the contact force is oscillating between zero and positive values, showing that the slider is only intermittently contacting the disk. This intermittent contact contributes to the slider's pitch motion at its second pitch mode, leading to the appearance of peaks at ~400kHz in the power spectrum. Note that the large spike at the very beginning of each actuation step in Figure 7 is due to the use of a step function as the actuation signal, so it does not represent a physical phenomenon.

When the actuation is further increased to 33nm, a much larger response appears at around 200kHz with the highest peak located at 195.3kHz, as shown in Figure 5.

Using the same procedure as described above, we obtained the pitch axis for this mode as shown in the Figure 6. The axis is located close to the trailing edge, and thus is considered to be the nodal line of the first air bearing pitch mode. By observing the history of the mean minimum FH (Figure 8), we find that the reduction rate of the minimum FH with increasing protrusion becomes smaller at around 33nm actuation. This is an indication that the interference between the slider's protruded part and the disk gets more pronounced, making it difficult for the slider to further reduce its flying-height. At this actuation step, the minimum of contact force shown in Figure 7 is greater than zero. Apparently, in this case the slider partially slides on the disk and pitches about the protruded area. The vibration amplitude is fairly large at the 1st pitch mode, showing the existence of unstable behavior at this actuation stage. A possible theoretical explanation for the excitation of the lower air bearing mode can be found in (Canchi and Bogy 2011).

As the actuation is further increased to 40nm, the largest response remains located at around 200kHz, with the frequency peak slightly moved to the right and the amplitude much suppressed compared with the case at 33nm actuation, as shown in Figure 5. This trend continues as the actuation is further increased to 45nm. The suppression in the vibration amplitude with increasing protrusion suggests that the unstable factors disappear at the over-pushed condition and a stable sliding state is established. The move of the peak to higher frequencies can be related to the increasing stiffness of the air bearing due to further compression of the air film.

## Conclusion

A numerical study is conducted to reveal the details of thermal flying-height control slider dynamics during the touchdown process. The general trend of the slider's motion predicted by the numerical simulation qualitatively agrees with experimental findings. The touchdown process begins with a slight intermittent contact between the slider's trailing edge and the disk, followed by a partial slider-disk contact at the trailing edge accompanied by a large pitch motion at the 1st air bearing mode; this pitch motion gets suppressed and the slider comes into stable sliding on the disk as the protrusion is further increased. The numerical approach used here provides a useful tool to study TFC slider's touchdown dynamics and improve sliders' performance at ultra-low flying clearance.

## References

Canchi, SV, Bogy,DB (2010) Slider Dynamics in the Lubricant-contact Regime. IEEE Trans Magn 46:764-769

Canchi, S, Bogy, DB(2011) Thermal flying-height control slider instability and dynamics at touchdown: explanations using nonlinear system theory. J Tribo. doi:10.1115/1.4003483

Chen, D, Bogy, DB(2007) Intermolecular force and surface roughness models for air bearing simulations for sub-5nm flying height sliders. Microsyst Technol 13: 1211-1217.

Chen, D, Bogy, DB(2007) Dynamics of partial contact head disk interface. IEEE Trans Magn 43:2220-2222

Stanley, HM, Etsion, I, Bogy, DB(1990) Adhesion of Contacting Rough Surfaces in the Presence of Sub-boundary Lubrication. J Tribo 112:98-104.

Su, L, Hu, Y, Lam, EL, Li, P, Ng, RW, Liang, D, Zheng O, Liu, H, Deng, Z, Zhang, J(2011) Tribological and Dynamic Study of Head Disk Interface at Sub-1-nm Clearance. IEEE Trans Magn 47:111-116

Zeng, Q, Yang, CH, Ka, S, Cha, E (2011) an Experimental and Simulation Study of Touch-down Dynamics. Proc IEEE Int Magn Conf

Zheng, J, Bogy, DB, Zhang, S, Yan, W(2009) Effects of altitude on the thermal flying height actuation ASME/STLE 2009 Int Jt Tribo Conf

Zheng J, Bogy DB (2010) Investigation of Flying-Height Stability of Thermal Fly-Height Control Sliders in Lubricant or Solid Contact with Roughness. Tribol Lett 38:283-289

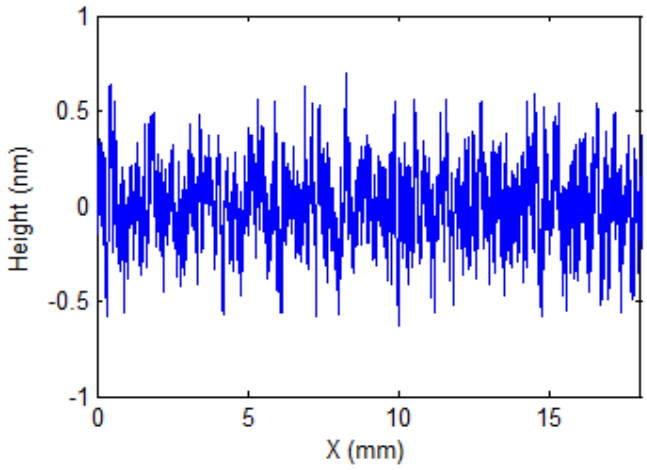


Figure 1 A 18mm LDV-measured disk profile

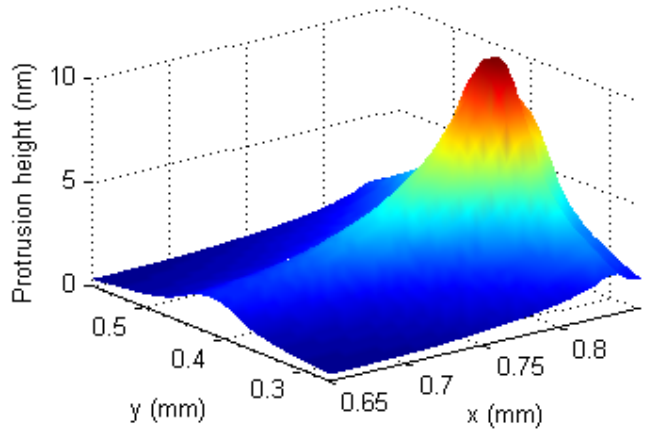


Figure 2 Heater-induced bulge profile with a peak of 10nm

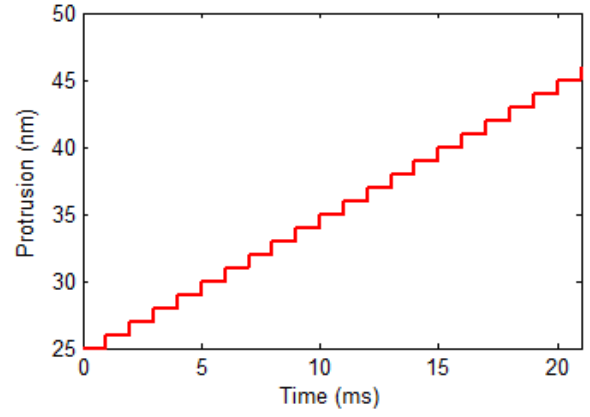


Figure 3 The actuation profile applied on the slider

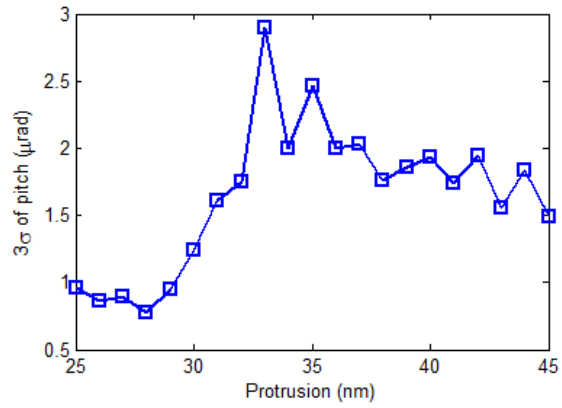


Figure 4 Variation of the slider's pitch 3σ with increasing protrusion

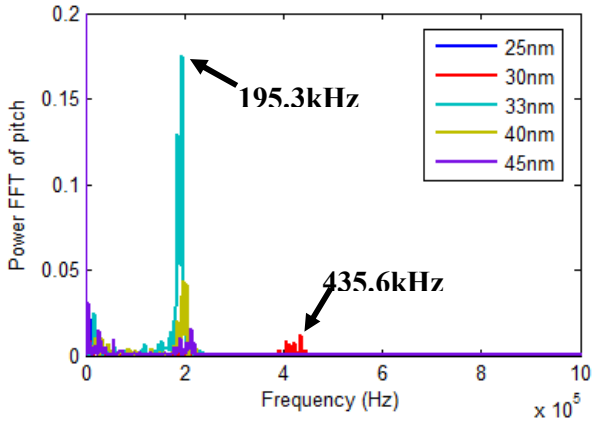


Figure 5 Power FFT of the slider's pitch history at 25nm, 30nm, 33nm, 40nm and 45nm actuations

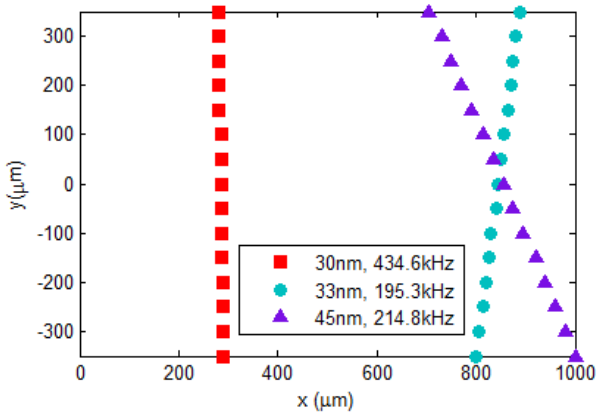


Figure 6 Nodal lines for the excited modes at different actuation stages

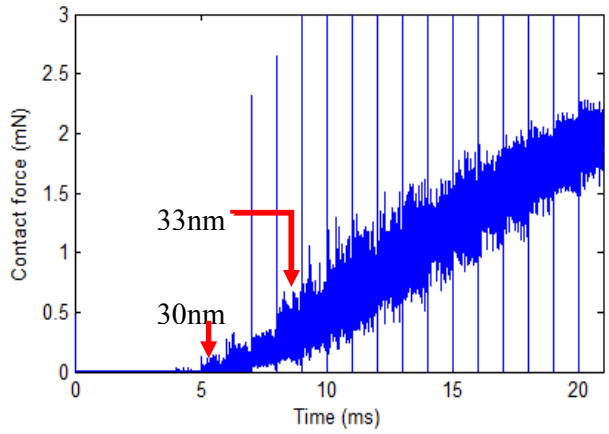


Figure 7 Time history of contact force

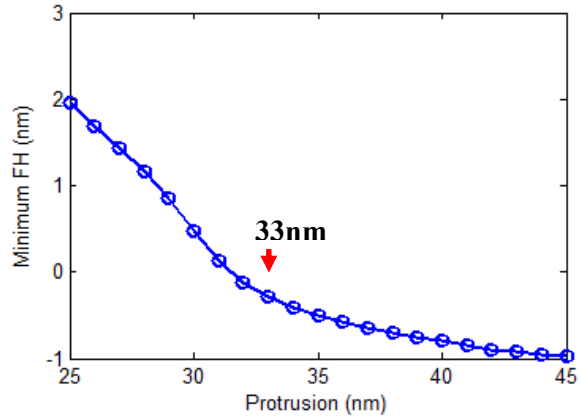


Figure 8 Variation of minimum FH with increasing actuation